

Three-phase Leidenfrost effect

Mojtaba Edalatpour ¹, Daniel T. Cusumano,² Saurabh Nath,^{2,3} and Jonathan B. Boreyko ^{1,2,*}

¹*Department of Mechanical Engineering, Virginia Tech, Blacksburg, Virginia 24061, USA*

²*Department of Biomedical Engineering and Mechanics, Virginia Tech, Blacksburg, Virginia 24061, USA*

³*Physique et Mécanique des Milieux Hétérogènes, UMR 7636 du CNRS, ESPCI, 75005 Paris, France*



(Received 23 October 2020; accepted 10 December 2021; published 21 January 2022)

To date, the Leidenfrost effect has been a two-phase phenomenon: either an evaporating liquid or a sublimating solid levitates on its vapor. Here, we demonstrate that an ice disk placed on a sufficiently hot surface exhibits a three-phase Leidenfrost effect, where both liquid and vapor films emanate from under the levitating ice. Curiously, the critical Leidenfrost temperature was about 400 °C hotter for ice than for a water drop. As a result, the effective heat flux was an order of magnitude larger when quenching aluminum with ice rather than water over a wide temperature range of 150–550 °C. An analytical model reveals the mechanism for the delayed film boiling: the majority of the surface's heat is conducted across the levitating meltwater film due to its 100 °C temperature differential, leaving little heat for evaporation.

DOI: [10.1103/PhysRevFluids.7.014004](https://doi.org/10.1103/PhysRevFluids.7.014004)

I. INTRODUCTION

The Leidenfrost effect, where a heated liquid levitates atop its own vapor, has been known for centuries but remains a rich field of study due to its surprising fluid flow phenomena [1–4]. A second form of the Leidenfrost effect, where a sublimating solid (ex: dry ice) levitates on its vapor, has also come into appreciation over the past decade in particular [5–8]. Notable fluid dynamical aspects of the Leidenfrost state include ultra-high mobility due to the lack of contact angle hysteresis [9], reduced hydrodynamic drag of a bluff body [10], special droplet shapes due to vapor-induced oscillations [11], out-of-plane takeoff at small droplet sizes [12], and rich modes of Rayleigh-Taylor and Rayleigh-Plateau instabilities [1,13]. In-plane self-propulsion is also possible, either by employing asymmetric surface structures to induce a directional vapor flow [14–16] or by exploiting the self-rotation of Leidenfrost drops due to the underlying vapor shear [17].

The Leidenfrost state may be on excellent terms with curious fluid dynamicists, but its insulating vapor film is undesirable for spray cooling applications in metallurgy [18], fire fighting [19], and preventing pressure buildup in nuclear reactors [20]. The critical temperature where nucleate boiling is completely replaced by film boiling, known as the Leidenfrost point [21–24], can be increased by using structured surfaces [22,25–31]. Surface structures can elevate the Leidenfrost point in at least two ways: by “poking” through the vapor layer to reclaim direct contact with the liquid [22,27–29], or by redirecting the vapor flow to prevent levitation [30]. Limitations to increasing the Leidenfrost point via surface modification include the poor durability and scalability of the complex micro-/nanostructures and a lack of applicability to scenarios such as firefighting where the surface is not known in advance. The Leidenfrost state can also be suppressed by an applied electric field [32], but this requires inserting an electrode into the droplet and is not conducive to spray cooling.

Here, we identify for the first time a three-phase Leidenfrost effect (Fig. 1), which exhibits an unprecedentedly high Leidenfrost point on a smooth surface. We define the three-phase Leidenfrost

*boreyko@vt.edu

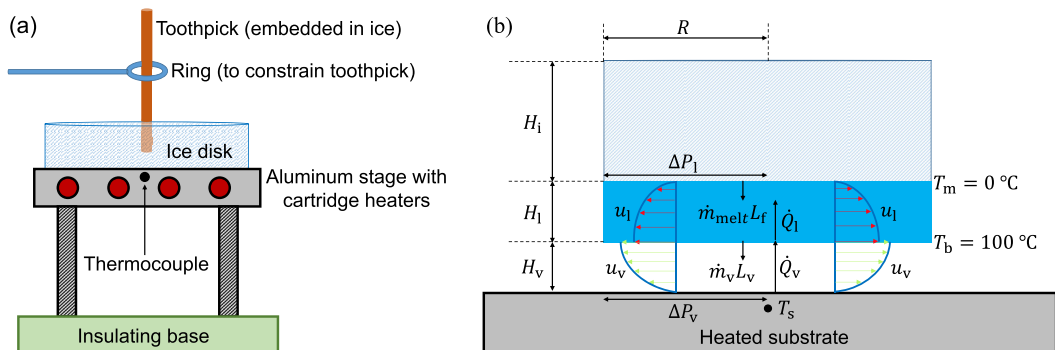


FIG. 1. (a) Schematic of the experimental setup. (b) Diagram of the three-phase Leidenfrost effect, where H_i , H_l , and H_v are the thicknesses of the ice disk, meltwater layer, and vapor layer, respectively. The solid-liquid interface is fixed at the melting temperature, $T_m = 0^\circ\text{C}$, while the liquid-vapor interface is at the boiling point, $T_b = 100^\circ\text{C}$. Radial semi-plug Couette flows are generated in the liquid layer (pressure gradient $\Delta P_l/R$, velocity u_l) and vapor layer ($\Delta P_v/R$, velocity u_v). A subset of the heat conducted across the vapor layer (\dot{Q}_v) is transferred into the liquid layer (\dot{Q}_1) to melt the ice ($\dot{m}_{\text{melt}}L_f$), while the remainder evaporates the meltwater (\dot{m}_vL_v).

effect as frozen water (i.e., ice) levitating on its meltwater, which in turn is levitating on its evaporative vapor. A few recent studies characterized the dynamics of melting ice disks on heated substrates [33] or water baths [34], but only up to 35°C . In contrast to liquid water, which exhibits a Leidenfrost point of $T_{\text{LP}} \approx 150^\circ\text{C}$ on a smooth aluminum surface [1], we observe a dramatic $T_{\text{LP}} \approx 550^\circ\text{C}$ for a disk of ice. An analytical model reveals that this dramatic stretching of the boiling curve is primarily due to most of the heat being conducted to the meltwater film.

II. EXPERIMENTAL METHODS

Polycarbonate petri dishes were filled with distilled water and frozen in a freezer to produce ice disks. The radius of each disk was either $R = 8\text{ mm}$ or 25 mm , while the thickness was either $H_i = 7\text{ mm}$ or 12 mm . The temperature of a smooth aluminum stage was measured by a thermocouple (Omega Engineering, TJ36-CAXL-032U-4), ranged from $T_s = 100\text{--}550^\circ\text{C}$ by increments of 25°C . The aluminum stage could not exceed 550°C , as it was observed that warping occurred near the melting point. To gently deposit the ice disks onto the heated aluminum stage, a toothpick was suspended into the top half of the water prior to freezing. To ensure that the ice disks did not glide off the stage, a ring constrained the toothpick's lateral motion. The lifetime of the ice phase (i.e., melting time) was measured with a side-view digital Canon EOS 5D Mark III camera. The ambient laboratory environment was room temperature for all experiments, such that the air's contribution to melting the ice was negligible compared to the heated aluminum stage. Even after the ice disk completely melted, some meltwater remained on the aluminum. However, the evaporation lifetime of the meltwater could not be measured, due to its high mobility. While the evaporation lifetime can easily be measured by machining an indentation into the heated stage [1], this was not possible in our case as it would interface with the rigid ice disk's interaction with the surface. For this reason, we focus here on the melting lifetime of the water and not the subsequent evaporation lifetime.

III. RESULTS AND DISCUSSION

Figure 2, as well as Videos S1–S4 in Ref. [35], depict the four temperature-dependent regimes observed when the ice disks were deposited on the superheated aluminum stage. The transition temperature between adjacent regimes has an uncertainty of about $\pm 25^\circ\text{C}$. A suppressed boiling

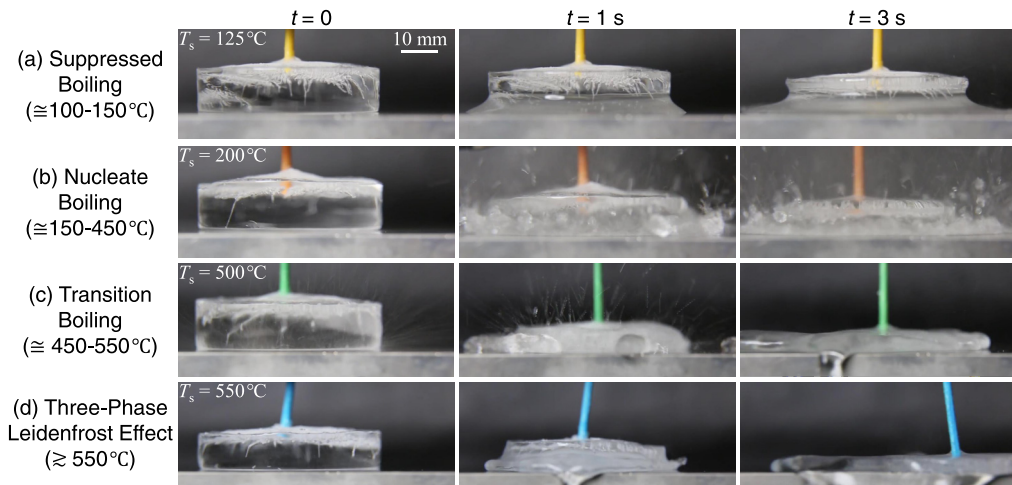


FIG. 2. Side-view imaging of an ice disk of initial radius $R = 25$ mm, height $H_i = 12$ mm, and volume $V = 23.56$ cm³ being placed on an aluminum stage heated to different temperatures. Four different regimes of heat transfer occurred depending on the temperature: (a) Suppressed boiling, (b) nucleate boiling, (c) transition boiling, and (d) three-phase Leidenfrost effect. See Figs. S2–S4 for equivalent imaging of the other three sizes of ice disks and Videos S1–S4 in Ref. [35] to see the dynamic melting of all of the ice disks.

regime was observed at moderate superheats ($100^\circ\text{C} < T_s < 150^\circ\text{C}$), where no nucleate boiling was visible within the film of meltwater beneath the ice. This is due to the presence of 0°C ice above the meltwater film, which effectively subcools the upper portion of the meltwater. While previous studies did not consider the present context of a three-phase system, it is more generally known that nucleated bubbles can spontaneously collapse once the surrounding water becomes subcooled [36]. After the ice completely melted, nucleate boiling was observed throughout the remaining meltwater as expected.

In the temperature range of $150^\circ\text{C} < T_s < 450^\circ\text{C}$, nucleate boiling visibly occurred even in the meltwater underneath the ice disk. However, the rigid roof provided by the ice disk constrained and collapsed most of the bubbles, such that nucleate boiling was much stronger in the meltwater extending just beyond the ice. The pressure of the trapped bubbles was sufficient to occasionally lift a portion of the ice disk into the air. This extended nucleate boiling regime is in sharp contrast to liquid water, which exhibits a Leidenfrost point of $T_{LP} \approx 150^\circ\text{C}$ on a smooth aluminum surface [1]. Interestingly, from $150^\circ\text{C} < T_s < 300^\circ\text{C}$, the Leidenfrost regime was still suppressed even after the ice had finished melting (aside from sprayed satellite droplets that did rebound in the Leidenfrost state). From the video footage, this appears to be because the meltwater preferentially spreads out into an evaporation-rich annular film that extends well beyond the ice, such that virtually no water remains after the completion of melting. From $300^\circ\text{C} < T_s < 450^\circ\text{C}$, there was enough water remaining after the ice had completely melted to assume the Leidenfrost state.

Moving into yet higher superheats ($450^\circ\text{C} < T_s < 550^\circ\text{C}$), transition boiling was observed. Nucleate boiling still occurred, but was noticeably calmer, indicating the partial presence of a vapor layer. The exact transition from nucleate to transition boiling was demarcated by an increase in melting lifetime with increasing temperature for the transition boiling regime. This surprising finding that nucleate and transition boiling regimes were able to persist even above 500°C indicates that ice stretches the boiling curve compared to the classic boiling curve for liquid water. This dramatic stretching of the boiling curve should be of practical interest for quenching applications, where it is desirable to retain nucleate boiling at higher temperatures [18–20]. After the ice completely melted, the centralized meltwater reverted to a classical Leidenfrost state analogous to that described for the upper-range of the nucleate boiling regime.

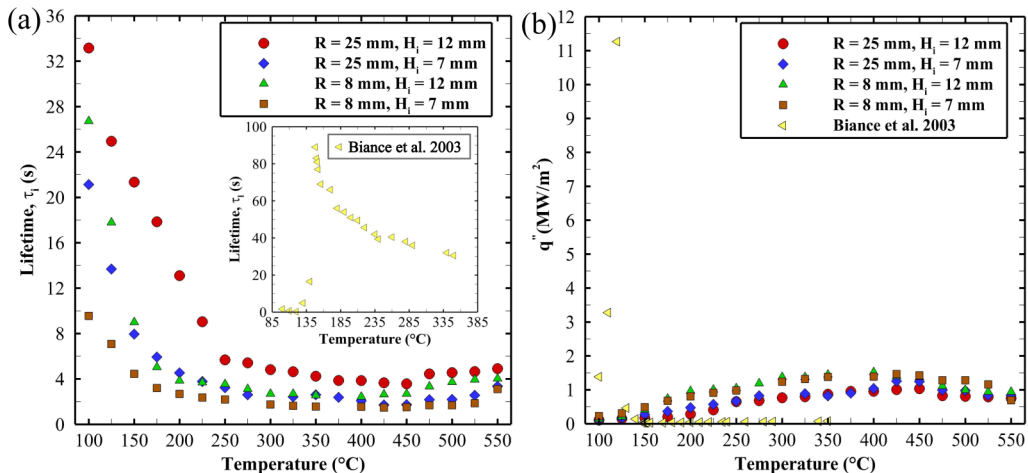


FIG. 3. (a) Melting lifetime of ice disks (τ_i) on an aluminum substrate, which the inset compares to the previously reported evaporation lifetimes of water droplets (τ_i) on an aluminum substrate (Bianco *et al.* 2003 [1]). (b) Effective heat flux supplied into the ice disks (q''_i) or water droplets (q''_l), as calculated from Eq. (1). See Fig. S5 in Ref. [35] for additional comparisons of τ_i and q''_i to those for water on a variety of surfaces [23,25,26,30,31].

Finally, the three-phase Leidenfrost effect was observed at the highest temperature range achievable with our setup (550°C). Using high-magnification side-view imaging, a continuous vapor layer was observed beneath the layer of meltwater (see Fig. S1 in Ref. [35]). The Leidenfrost state was further evidenced by the complete lack of nucleate boiling, both in the meltwater film underneath the ice and also in expelled meltwater droplets. To our knowledge, this is the first reported instance of having composite liquid and vapor films extending continuously beneath a melting solid, i.e., a three-phase Leidenfrost effect. It is remarkable that the three-phase Leidenfrost point is approximately $T_{LP} \approx 550^{\circ}\text{C}$, considering that this is 400°C above the Leidenfrost point for water droplets [1] and prior works have shown that the extent of subcooling does not appreciably increase the Leidenfrost point for liquid droplets [22,37].

In Fig. 3(a), the melting lifetime (τ_i) of the ice disks was plotted as a function of T_s . In sharp contrast to water droplets [Fig. 3(a) inset], where the evaporation lifetime τ_i increased by a factor of 500 upon reaching T_{LP} [1], the ice disks only exhibited decreasing values of τ_i that plateaued around 300°C to a fairly stable value. While there was the expected increase in τ_i upon entering the transition and film boiling regimes, the increase was quite weak (factor of ≈ 2). The post-melting lifetime of the water was $\tau_i \rightarrow 0$ s from $100^{\circ}\text{C} < T_s < 300^{\circ}\text{C}$, due to the aforementioned thin-film nucleate boiling of the meltwater. While τ_i could not be measured for $T_s > 300^{\circ}\text{C}$ due to the meltwater sliding off the stage in the mobile Leidenfrost state, $\tau_i \gg \tau_i$ would be expected due to onset of film boiling and the latent heat of vaporization being about seven times larger than the latent heat of melting.

Using the measured values of τ_i and the known mass and area of the ice disks, the effective heat flux entering the ice disks is calculated in Fig. 3(b):

$$q''_i \approx \rho_i H_i L_f / \tau_i, \quad (1)$$

where $\rho_i = 917 \text{ kg}/\text{m}^3$ is the density of ice at 0°C , $L_f = 334 \text{ kJ}/\text{kg}$ is the latent heat of fusion, and the cross-sectional area of the ice disk was assumed to be roughly constant as the ice melted. As a control, the effective heat flux of water droplets is analogously calculated using $q''_l \sim \rho_l R L_v / \tau_l$, where $\rho_l = 958 \text{ kg}/\text{m}^3$ is the density of water at 100°C , R is the initial radius of the quasi-spherical droplet, $L_v = 2,260 \text{ kJ}/\text{kg}$ is the latent heat of vaporization, and τ_l is the evaporation lifetime of

$V = 4.19 \text{ mm}^3$ water droplets measured from Ref. [1]. This calculation is more crude than that for ice, as the droplet's contact area with the substrate shrinks over time, but should suffice for a scaling estimate. Interestingly, when comparing q_i'' to q_1'' , two opposing trends are revealed. For superheats beneath the Leidenfrost point for water, $q_i'' \ll q_1''$, due to the aforementioned suppression of nucleate boiling beneath the ice. However, for superheats above the water's Leidenfrost point, $q_i'' \gg q_1''$, as now nucleate/transition boiling is exclusive to the ice. For example, when comparing water and ice on a smooth aluminum surface, a large ratio of $q_i''/q_1'' \approx 19$ is obtained at 350°C . This large ratio is impressive when considering that the heat flux entering the ice is only a subset of the aluminum surface's heat flux, as it does not account for additional heat used for evaporation. As described above, from $300^\circ\text{C} < T_s < 550^\circ\text{C}$, this enhancement in heat flux will only last for the lifetime of the ice, beyond which the water reverts to the Leidenfrost state.

The curiously high Leidenfrost temperature for ice can be rationalized by coupling the heat transfer, latent heat, and semiplug Couette flow equations of the three-phase Leidenfrost regime. Consider an ice disk of radius R and initial thickness H_1 . The temperature difference across the thin underlying film of levitating liquid is $\Delta T_1 = T_b - T_m = 100^\circ\text{C}$ where T_b and T_m are the boiling and melting points, respectively. It is an open question whether the heat transfer across this liquid film is primarily conductive or convective in nature. One possibility for the heat transfer across the meltwater film is Rayleigh-Bénard convection due to thermal buoyancy [38]. The Rayleigh number compares the thermal buoyancy and viscosity of a fluid: $\text{Ra} = \rho_1 g \beta_1 H_1^3 \Delta T_1 / (\alpha_1 \mu_1)$, where g is gravity, β_1 is the thermal expansion coefficient, H_1 is the liquid film thickness, α_1 is the thermal diffusivity, and μ_1 is the dynamic viscosity. The Prandtl number, which compares the ratio of momentum diffusivity to thermal diffusivity and is given by $\text{Pr} = \nu_1 / \alpha_1$ (where ν_1 is the kinematic viscosity), also affects the nature of the Rayleigh-Bénard convection. For typical values corresponding to our range of experimental conditions, here we have $\text{Ra} \sim 10$, $\text{Pr} \approx 3.4$, and $\Gamma \sim 100$, where Γ is the aspect ratio. This value of Ra , while greater than unity, is actually quite negligible in the context of critical Rayleigh-Bénard convection. For example, for a square cavity where $\Gamma = 1$, buoyancy is generally unable to overcome viscous stresses beneath a critical value of $\text{Ra}_c \approx 1,708$ [39]. Therefore, it seems unlikely that the dominant mode of heat transfer is Rayleigh-Bénard convection in the meltwater film, although it could be playing a secondary role. Bénard-Marangoni convection also seems unlikely [40,41], as the fluid-fluid interface exhibits film boiling and should therefore exhibit a fairly uniform temperature of about 100°C . Convection due to radial flow in the liquid layer is also expected to be negligible (see Supplemental Material [35]).

Therefore, we expect that heat transfer across the meltwater film is primarily conductive:

$$\dot{Q}_1 = \frac{\pi R^2 k_1 \Delta T_1}{H_1}, \quad (2)$$

where k_1 is the thermal conductivity of liquid water. Heat transfer was assumed to be negligible along the side walls or top of the ice disk. The mass flow rate of ice melting is $\dot{m}_{\text{melt}} = \dot{Q}_1 / L_f$. Given that $H_1 \ll R$, we invoke the lubrication approximation and assume a radial semi-plug Couette flow in the liquid film:

$$\dot{m}_1 = \dot{m}_{\text{melt}} - \dot{m}_v = \frac{2\pi \rho_1 H_1^3 \Delta P_1}{3\mu_1}, \quad (3)$$

where \dot{m}_v is the mass flow rate of the evaporative vapor. The pressure exerted on the liquid film is caused by the weight of the overlying ice disk and also by the average hydrostatic pressure of the meltwater itself:

$$\Delta P_1 = g \left(\rho_1 H_i + \frac{1}{2} \rho_1 H_1 \right), \quad (4)$$

Now consider the underlying vapor film of unknown thickness H_v , which must exhibit a temperature gradient of $\Delta T_v = T_s - T_b$. Neglecting radiation, which is smaller than conduction for

$T_s < 1,000^\circ\text{C}$ [4], the conductive heat transfer across the vapor layer is

$$\dot{Q}_v = \frac{\pi R^2 k_v \Delta T_v}{H_v}, \quad (5)$$

where k_v is the thermal conductivity of water vapor. For a classical two-phase Leidenfrost state, \dot{Q}_v is wholly devoted to evaporation at the liquid-vapor interface [1]. In sharp contrast, here a portion of \dot{Q}_v is also being transferred by conduction across the additional liquid film to maintain ΔT_1 :

$$\dot{m}_v = \frac{\dot{Q}_v - \dot{Q}_l}{L_v}. \quad (6)$$

Similar to the liquid film, we assume a radial semiplug Couette flow as $H_v \ll R$,

$$\dot{m}_v = \frac{2\pi \rho_v H_v^3 \Delta P_v}{3\mu_v}, \quad (7)$$

where ρ_v and μ_v are the density and viscosity of water vapor. The pressure is caused by the joint weight of the ice plus the water film:

$$\Delta P_v = g(\rho_i H_i + \rho_l H_l). \quad (8)$$

The governing equation for the liquid film is obtained by combining Eqs. (2)–(6):

$$\frac{k_l \Delta T_1}{H_l} \left(\frac{L_f + L_v}{L_f L_v} \right) - \frac{k_v \Delta T_v}{L_v H_v} - \frac{2\rho_l H_l^3 \Delta P_l}{3R^2 \mu_l} = 0, \quad (9)$$

where H_l and H_v are unknowns. The accompanying equation for the vapor film, with the same two unknowns, is constructed from Eq. (2) and Eqs. (5)–(8):

$$\frac{k_v \Delta T_v}{H_v} - \frac{k_l \Delta T_1}{H_l} - \frac{2\rho_v L_v H_v^3 \Delta P_v}{3R^2 \mu_v} = 0. \quad (10)$$

Solving Eqs. (9) and (10) simultaneously, we can now estimate the characteristic thicknesses of H_l and H_v for the three-phase Leidenfrost regime. A surface temperature of $T_s = 550^\circ\text{C}$ was chosen to correspond to the Leidenfrost point for all ice disks used. The thermophysical properties corresponded to the average temperature of the liquid $[(T_b + T_m)/2]$ and vapor $[(T_s + T_b)/2]$ layers. These assumptions result in film thicknesses with order-of-magnitude scaling values of $H_l \sim 100 \mu\text{m}$ and $H_v \sim 10 \mu\text{m}$ for all four ice pucks used here. This is in good agreement with the vapor film beneath classical Leidenfrost drops, which similarly scales as $H_v \sim 10 \mu\text{m}$ for mid-sized droplets [1]. The exact film thicknesses will of course depend on the initial dimensions of the ice puck, vary in time as the ice melts, and vary radially due to buoyancy effects. However, the scaling values calculated here are reasonable characteristic values of the film thicknesses across the lifetime of any given ice puck. Future studies could utilize a transparent sapphire substrate to facilitate direct measurements of the vapor and liquid film thickness, how it varies radially [3,42], and whether the Rayleigh-Taylor instability could thin the confined liquid film [13].

By plugging the characteristic film thicknesses calculated from Eqs. (9) and (10) back into Eqs. (2) and (5), we can predict the heat fluxes across the liquid (q_l'') and vapor (q_v'') layers, respectively. These theoretical heat flux values are graphed in Fig. 4(a), alongside the experimental estimation of q_l'' obtained from the measurement of the melting lifetime (at $T_s = 550^\circ\text{C}$) being plugged into Eq. (1). Note that the heat flux across the liquid layer is equivalent to the heat flux entering into (i.e., melting) the ice disk, such that $q_l'' \approx q_i''$. Across all four ice disks, the theoretical prediction of $q_l'' \approx 0.64 \text{ MW/m}^2$ agrees with the experimental estimations of q_l'' to within 32% or less. Importantly, \dot{Q}_l is approximately 69% of \dot{Q}_v , revealing that the majority of the heat conducted across the vapor layer is subsequently conducted across the liquid layer. Therefore, conduction across the liquid meltwater dominates at the expense of evaporation at the liquid-vapor interface (i.e., $\dot{Q}_v - \dot{Q}_l$). In contrast, virtually all of the heat conducted across the vapor layer is used for

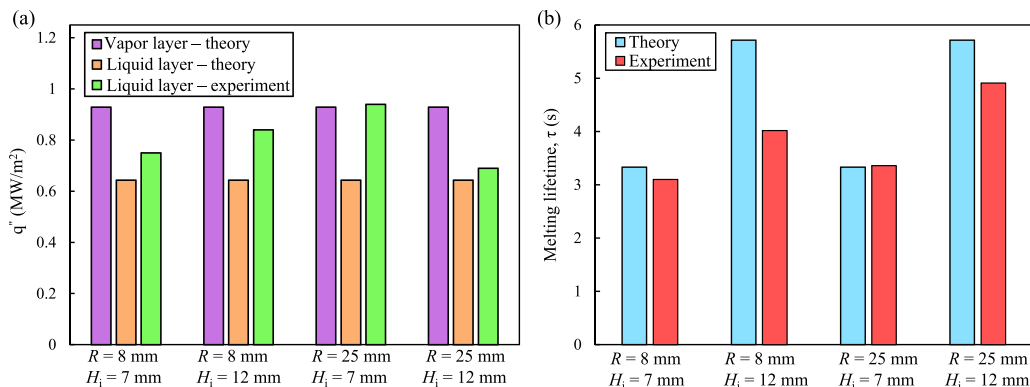


FIG. 4. (a) Theoretical estimation of the heat fluxes conducted across the vapor layer [Eq. (5)] and meltwater layer [Eq. (2)], for ice disks exhibiting the three-phase Leidenfrost effect at $T_s = 550^\circ\text{C}$. The theoretical q'' is compared against the experimental approximation, obtained by plugging the measured τ_i into Eq. (1). (b) Comparison of the theoretical and experimental values of τ_i , again for the case of the three-phase Leidenfrost effect at $T_s = 550^\circ\text{C}$. The theoretical τ_i is obtained by plugging the prediction for q'' into Eq. (1).

evaporation in the conventional case of a liquid droplet [1]. This fundamental difference between the two-phase and three-phase Leidenfrost effects rationalizes the extraordinarily large Leidenfrost point for the latter case.

The theoretical prediction of the melting lifetime of each ice disk is obtained by plugging the theoretical $q''_l \approx q''_i$ into Eq. (1) and solving for τ_i . Note that this is the inverse of the experimental case, where τ_i was measured directly and plugged into Eq. (1) to estimate q''_i . The comparison of the theoretical and experimental τ_i values are graphed in Fig. 4(b). For the smaller ice disk thickness ($H_i = 7$ mm), the theoretical τ_i agrees with the experimental one to within 8%. For the larger ice disk thickness ($H_i = 12$ mm), the theoretical melting lifetime shows a roughly 42% error against the experimental measurements. This is still a quite reasonable agreement, especially considering the inherent uncertainty in modeling of the three-phase Leidenfrost effect and the model's many simplifying assumptions: a fixed R for liquid/vapor films over time, spatially uniform film thicknesses (neglecting buoyancy), and using averaged thermophysical properties.

There are important distinctions between our approach of using ice versus using water subcooled to 0°C . When a 0°C droplet of radius $R \sim 1$ mm is deposited on a surface heated above T_{LP} , the time required for the entire Leidenfrost droplet to reach 100°C scales as $\tau \sim R^2/\alpha_l \approx 6$ s. This estimate is extremely conservative, as it neglects internal convection [17] and the common reality of transient nucleate boiling upon initial droplet contact [42]. Regardless, this warming timescale is an order of magnitude smaller than the lifetime of a Leidenfrost droplet, such that the substrate's heat is predominantly used to overcome latent heat of vaporization for the large majority of the time. During the initial warming stage, where some heat is being diverted for sensible heating, critically this does not appreciably increase the Leidenfrost point [22,37]. We suggest three reasons why diverting heat into the ice, but not subcooled water alone, can uniquely and dramatically raise the Leidenfrost point. First, although in both cases the temperature gradient across the liquid phase is initially $\sim 100^\circ\text{C}$, the meltwater film beneath ice is microscopic whereas the bulk liquid droplet is millimetric. This results in at least an order-of-magnitude enhancement in the amount of heat conducted into the liquid for the case of a three-phase system. Second, the $\sim 100^\circ\text{C}$ temperature differential is maintained when using ice as a phase change material, whereas it would decrease over time when using water alone. Third, the ice roof serves to constrain and collapse vapor bubbles to further suppress film boiling, to complement the diversion of heat away from the evaporating interface.

IV. CONCLUSION

In conclusion, we have shown for the first time that depositing a disk of ice onto a sufficiently heated surface produces a solid-liquid-vapor triple stack, which we coin the three-phase Leidenfrost effect. The Leidenfrost point for ice is approximately 550°C on a smooth aluminum surface, a dramatic increase compared to the approximately 150°C required to levitate a water droplet on the same surface. A theoretical model revealed that the increased Leidenfrost point is due to the majority of the surface's heat getting conducted across the thin meltwater film that inherently exhibits a fixed 100°C temperature differential, leaving only a fraction ($\approx 31\%$) leftover for evaporation. In contrast, a liquid droplet utilizes the large majority of the surface's heat for evaporation, resulting in the much lower Leidenfrost point. Practically, our finding that ice can suppress the Leidenfrost effect even at very large superheats suggests that using ice particles, rather than liquid droplets, may be a superior option for spray quenching applications. Analogous to using a structured substrate to delay film boiling for liquid droplets [22,25–31], we expect that the use of roughened and curved ice particles will even further suppress the Leidenfrost state compared to our smooth and flat ice disks, which we encourage as an avenue of future research. The three-phase Leidenfrost state should also be possible for other substances besides water, provided the pressure exceeds that of the triple point. It would also be interesting to explore the inverted Leidenfrost effect [10,43] in this new context of a three-phase system, by dropping hot spheres into ice baths or onto a solid sheet of ice.

ACKNOWLEDGMENTS

This work was supported by startup funds from the Department of Biomedical Engineering and Mechanics at Virginia Tech. We thank Mark Paul, Rui Qiao, Pengtao Yue, Danesh Tafti, and Farzad Ahmadi for fruitful discussions. We also thank the anonymous reviewers, who collectively helped us rule out Rayleigh-Bénard and Bénard-Marangoni convection as the primary heat transfer mechanisms and corrected a couple of faulty assumptions in our initial model.

-
- [1] A. L. Bianco, C. Clanet, and D. Quéré, Leidenfrost drops, *Phys. Fluids* **15**, 1632 (2003).
 - [2] A. L. Bianco, F. Chevy, C. Clanet, G. Lagubeau, and D. Quéré, On the elasticity of an inertial liquid shock, *J. Fluid Mech.* **554**, 47 (2006).
 - [3] J. C. Burton, A. L. Sharpe, R. C. A. van der Veen, A. Franco, and S. R. Nagel, Geometry of the Vapor Layer Under a Leidenfrost Drop, *Phys. Rev. Lett.* **109**, 074301 (2012).
 - [4] D. Quéré, Leidenfrost dynamics, *Annu. Rev. Fluid Mech.* **45**, 197 (2013).
 - [5] G. Dupeux, M. Le Merrer, G. Lagubeau, C. Clanet, S. Hardt, and D. Quéré, Viscous mechanism for Leidenfrost propulsion on a ratchet, *Europhys. Lett.* **96**, 58001 (2011).
 - [6] G. Dupeux, T. Baier, V. Bacot, S. Hardt, C. Clanet, and D. Quéré, Self-propelling uneven Leidenfrost solids, *Phys. Fluids* **25**, 051704 (2013).
 - [7] C. Antonini, I. Bernagozzi, S. Jung, D. Poulikakos, and M. Marengo, Water Drops Dancing on Ice: How Sublimation Leads to Drop Rebound, *Phys. Rev. Lett.* **111**, 014501 (2013).
 - [8] G. G. Wells, R. Ledesma-Aguilar, G. McHale, and K. Sefiane, A sublimation heat engine, *Nat. Commun.* **6**, 6390 (2014).
 - [9] G. Dupeux, M. Le Merrer, C. Clanet, and D. Quéré, Trapping Leidenfrost Drops with Crenulations, *Phys. Rev. Lett.* **107**, 114503 (2011).
 - [10] I. U. Vakarelski, J. O. Marston, D. Y. C. Chan, and S. T. Thoroddsen, Drag Reduction by Leidenfrost Vapor Layers, *Phys. Rev. Lett.* **106**, 214501 (2011).
 - [11] F. Celestini, T. Frisch, A. Cohen, C. Raufaste, L. Duchemin, and Y. Pomeau, Two-dimensional Leidenfrost droplets in a Hele-Shaw cell, *Phys. Fluids* **26**, 032103 (2014).
 - [12] S. Lyu, V. Mathai, Y. Wang, B. Sobac, P. Colinet, D. Lohse, and C. Sun, Final fate of a Leidenfrost droplet: Explosion or takeoff, *Sci. Adv.* **5**, eaav8081 (2019).

- [13] P. S. Raux, G. Dupeux, C. Clanet, and D. Quéré, Successive instabilities of confined Leidenfrost puddles, *Europhys. Lett.* **112**, 26002 (2015).
- [14] H. Linke, B. J. Alemán, L. D. Melling, M. J. Taormina, M. J. Francis, C. C. Dow-Hygelund, V. Narayanan, R. P. Taylor, and A. Stout, Self-Propelled Leidenfrost Droplets, *Phys. Rev. Lett.* **96**, 154502 (2006).
- [15] G. Lagubeau, M. Le Merrer, C. Clanet, and D. Quéré, Leidenfrost on a ratchet, *Nat. Phys.* **7**, 395 (2011).
- [16] R. L. Agapov, J. B. Boreyko, D. P. Briggs, B. R. Srijanto, S. T. Retterer, C. P. Collier, and N. V. Lavrik, Length scale of Leidenfrost ratchet switches droplet directionality, *Nanoscale* **6**, 9293 (2014).
- [17] A. Bouillant, T. Mouterde, P. Bourriane, A. Lagarde, C. Clanet, and D. Quéré, Leidenfrost wheels, *Nat. Phys.* **14**, 1188 (2018).
- [18] J. D. Bernardin and I. Mudawar, Validation of the quench factor technique in predicting hardness in heat treatable aluminum alloys, *Int. J. Heat Mass Transfer* **38**, 863 (1995).
- [19] G. Grant, J. Brenton, and D. Drysdale, Fire suppression by water sprays, *Prog. Energy Combust. Sci.* **26**, 79 (2000).
- [20] H. van Dam, Physics of nuclear reactor safety, *Rep. Prog. Phys.* **55**, 2025 (1992).
- [21] B. S. Gottfried, C. J. Lee, and K. J. Bell, The Leidenfrost phenomenon: Film boiling of liquid droplets on a flat plate, *Int. J. Heat Mass Transfer* **9**, 1167 (1966).
- [22] J. D. Bernardin and I. Mudawar, The Leidenfrost point: Experimental study and assessment of existing models, *J. Heat Transfer* **121**, 894 (1999).
- [23] S. H. Kim, H. S. Ahn, J. Kim, M. Kaviani, and M. H. Kim, Dynamics of water droplet on a heated nanotubes surface, *Appl. Phys. Lett.* **102**, 233901 (2013).
- [24] M. Shirota, M. A. J. van Limbeek, C. Sun, A. Prosperetti, and D. Lohse, Dynamic Leidenfrost Effect: Relevant Time and Length Scales, *Phys. Rev. Lett.* **116**, 064501 (2016).
- [25] H. Kim, B. Truong, J. Buongiorno, and L. Hu, On the effect of surface roughness height, wettability, and nanoporosity on Leidenfrost phenomena, *Appl. Phys. Lett.* **98**, 083121 (2011).
- [26] C. Kruse, T. Anderson, C. Wilson, C. Zuhlke, D. Alexander, G. Gogos, and S. Ndao, Extraordinary shifts of the Leidenfrost temperature from multiscale micro/nanostructured surfaces, *Langmuir* **29**, 9798 (2013).
- [27] C. T. Avedisian and J. Koplik, Leidenfrost boiling of methanol droplets on hot porous/ceramic surfaces, *Int. J. Heat Mass Transfer* **30**, 379 (1987).
- [28] D. A. del Cerro, A. G. Marín, G. R. B. E. Römer, B. Pathiraj, D. Lohse, and A. J. H. in't Veld, Leidenfrost point reduction on micropatterned metallic surfaces, *Langmuir* **28**, 15106 (2012).
- [29] H. M. Kwon, J. C. Bird, and K. K. Varanasi, Increasing Leidenfrost point using micro-nano hierarchical surface structures, *Appl. Phys. Lett.* **103**, 201601 (2013).
- [30] N. Farokhnia, S. M. Sajadi, P. Irajizad, and H. Ghasemi, Decoupled hierarchical structures for suppression of Leidenfrost phenomenon, *Langmuir* **33**, 2541 (2017).
- [31] G. C. Lee, J. Y. Kang, H. S. Park, K. Moriyama, S. H. Kim, and M. H. Kim, Induced liquid-solid contact via micro/nano multiscale texture on a surface and its effect on the Leidenfrost temperature, *Exp. Therm. Fluid Sci.* **84**, 156 (2017).
- [32] A. Shahriari, O. Ozkan, and V. Bahadur, Electrostatic suppression of the Leidenfrost state on liquid substrates, *Langmuir* **33**, 13207 (2017).
- [33] S. Dorbolo, N. Vandewalle, and B. D. Texier, Spontaneous rotation of an ice disk while melting on a solid plate, *Phys. Fluids* **28**, 123601 (2016).
- [34] A. J. Schwartz and G. H. Pollack, Ice-melting dynamics: The role of protons and interfacial geometry, *Langmuir* **33**, 5585 (2017).
- [35] See Supplemental Material at <http://link.aps.org/supplemental/10.1103/PhysRevFluids.7.014004> for additional experimental results and videos on how ice stretches the boiling curve.
- [36] C. F. Gomez, C. W. M. van der Geld, J. G. M. Kuerten, R. Liew, M. Bsibsi, and B. P. M. van Esch, The nature of boiling during rewetting of surfaces at temperatures exceeding the thermodynamic limit for water superheat, *J. Fluid Mech.* **895**, A3 (2020).
- [37] K. J. Baumeister, R. E. Henry, and F. F. Simon, Role of the surface in the measurement of the Leidenfrost temperature, Technical Report, NASA, E-5828 (1970).
- [38] S. Grossmann and D. Lohse, Scaling in thermal convection: A unifying theory, *J. Fluid Mech.* **407**, 27 (2000).

- [39] F. P. Incropera and D. P. DeWitt, *Introduction to Heat Transfer* (John Wiley & Sons, New York, NY, 2002).
- [40] D. Johnson and R. Narayanan, A tutorial on the Rayleigh-Marangoni-Bénard problem with multiple layers and side wall effects, [Chaos](#) **9**, 124 (1999).
- [41] T. Boeck and A. Thess, Power-law scaling in Bénard-Marangoni convection at large Prandtl numbers, [Phys. Rev. E](#) **64**, 027303 (2001).
- [42] T. Tran, H. J. J. Staat, A. Prosperetti, C. Sun, and D. Lohse, Drop Impact on Superheated Surfaces, [Phys. Rev. Lett.](#) **108**, 036101 (2012).
- [43] I. U. Vakarelski, N. A. Patankar, J. O. Marston, D. Y. C. Chan, and S. T. Thoroddsen, Stabilization of Leidenfrost vapour layer by textured superhydrophobic surfaces, [Nature](#) **489**, 274 (2012).